Assembly of Aβ Amyloid Protofibrils: An in Vitro Model for a Possible Early Event in Alzheimer's Disease[†]

James D. Harper,[‡] Stanislaus S. Wong,[§] Charles M. Lieber,*[,§] and Peter T. Lansbury, Jr.*[,‡]

Center for Neurologic Diseases, Brigham and Women's Hospital and Department of Neurology, Harvard Medical School, Harvard Institutes of Medicine Building, 77 Avenue Louis Pasteur, Boston, Massachusetts 02115, and Department of Chemistry and Chemical Biology, Harvard University, 12 Oxford Street, Cambridge, Massachusetts 02138

Received February 22, 1999; Revised Manuscript Received May 3, 1999

ABSTRACT: Amyloid fibrils comprising primarily the peptides Aβ40 and Aβ42 are a defining feature of the Alzheimer's disease (AD) brain, and convergent evidence suggests that the process of their formation plays a central role in the AD pathogenic pathway. Elucidation of fibril assembly is critical for the discovery of potential AD diagnostics and therapeutics, since the pathogenic entity is not necessarily the product fibril, but could be a precursor species whose formation is linked to fibrillogenesis in vivo. Atomic force microscopy allowed the identification of an unanticipated intermediate in in vitro fibril formation, the Aβ amyloid protofibril. This manuscript describes studies of the structure of the Aβ40 protofibril and its in vitro assembly and disassembly using atomic force microscopy (AFM). The Aβ40 protofibril has a height of ca. 4.3 ± 0.5 nm and a periodicity of ca. 20 ± 4.7 nm. The rate of its elongation depends on the total concentration of Aβ40, the temperature, and ionic strength of the medium. Aβ42 and Aβ40 protofibrils elongate at a comparable rate. Statistical analysis of AFM data reveals a decrease in the number of protofibrils with time, indicating that coalescence of smaller protofibrils contributes to protofibril elongation. Similar analysis reveals that protofibrils shorten while the number of protofibrils also decrease following dilution, indicating that protofibril disassembly does not proceed by a reverse of the assembly process. These investigations provide systematic data defining factors affecting Aβ fibrillization and, thus, should be valuable in the design of high-throughput assays to identify agents which alter Aβ protofibril assembly.

Cortical amyloid plaques, comprising a fibrillar form of the amyloid-β protein (Aβ),[1] are the defining pathological feature of the Alzheimer's disease (AD) brain (*1*). The observation of amyloid plaques in the postmortem brain becomes more prevalent with age in AD patients and in cognitively normal individuals (*2*), although the number of plaques in the former population is far greater. In fact, the number of cortical amyloid plaques at autopsy roughly correlates with the severity of AD symptoms (*3*). In addition, the brains of Down syndrome patients, who invariably develop clinical AD in their thirties or forties, are characterized by abnormal Aβ deposits at an early age (*2, 4*). Taken together, these pathological observations suggest that amyloid fibril formation is an early and required event in the AD disease process (*5*). Genetic studies support this notion. Early-onset familial AD has been linked to three genes: the amyloid precursor protein and presenilins 1 and 2. All of these mutations increase the production of the faster-nucleating Aβ variant Aβ42 (*6*), consistent with the acceleration of amyloid fibril formation being critical (*5*). Two risk factors for development of late-onset AD also influence amyloid formation. ApoE genotype, a determinant of age of onset of sporadic AD (*7*), influences the level of amyloid deposition, such that the high-risk genotype (apoE4/4) is correlated with the most extensive amyloid deposition (*8*−*10*). In addition, head trauma, known to be a significant risk factor for the later development of AD, produces a transient and selective elevation of Aβ42 production (*11, 12*).

Since genetic factors that cause AD or increase susceptibility to AD also promote amyloid formation, inhibition of the formation of amyloid fibrils may have therapeutic benefit. However, if the pathogenic species is a precursor or an alternative to the fibril, then blocking fibril formation at too late a stage could accelerate disease by causing the toxic precursor to accumulate (*13*). It is therefore critical to elucidate the molecular mechanism of the fibril assembly process and to determine which species is responsible for pathogenesis (*14, 15*). An effective therapeutic agent targeting the amyloid formation process should act upstream of the pathogenic species to either halt further aggregation or promote the formation of benign oligomers (*15*). Since amyloid fibrils produced in vitro from synthetic Aβ variants

[†] This work was supported by a grant to C.M.L. and P.T.L. from the National Institute on Aging (PO1 AG14366). S.S.W. was supported by a fellowship from the Natural Sciences and Engineering Council of Canada.

* To whom correspondence should be addressed. (C.M.L.) Phone: (617) 496-3169. Fax: (617) 496-5442. E-mail: cml@cmliris.harvard.edu. (P.T.L.) Phone: (617) 525-5260. Fax: (617) 525-5252. E-mail: lansbury@cnd.bwh.harvard.edu.

[‡] Center for Neurologic Diseases.

[§] Department of Chemistry and Chemical Biology.

[1] Abbreviations: Aβ, amyloid-β protein; AD, Alzheimer's disease; ADDL's, Aβ-derived diffusible ligands; AFM, atomic force microscopy; DMSO, dimethyl sulfoxide; HOPG, highly ordered pyrolytic graphite; IAPP, islet amyloid polypeptide; LTP, long-term potentiation; MES, 2-(*N*-morpholino)ethanesulfonic acid; QLS, quasielastic light scattering.

10.1021/bi9904149 CCC: $18.00 © 1999 American Chemical Society
Published on Web 06/18/1999

resemble those extracted from AD brain, in vitro studies can provide relevant information about the in vivo process (*1*). Amyloid fibril formation is an ordered polymerization characterized by a slow nucleation, followed by rapid growth (*16*, *17*). Atomic force microscopy (AFM) has been utilized to probe the early events in the process (*13*, *18*−*21*). Using conventional silicon tip technology, this technique is capable of routinely providing ca. 10−20 nanometer resolution three-dimensional information about species that are adsorbed to an atomically smooth surface such as mica (*19*, *20*, *22*, *23*). Recent advances in the assembly and use of carbon nanotube AFM tips can improve resolution by an order of magnitude, into the ca. 1 nm range (*20*). The observation of individual adsorbed assemblies allows the construction of mechanistic models that stimulate experiments using complementary techniques (*18*, *24*).

Our preliminary AFM studies revealed the existence of a discrete, dynamic intermediate in Aβ fibril formation, which we designated the amyloid protofibril (*19*). Oligomeric Aβ species that are probably identical to those observed by AFM have also been observed by analytical ultracentrifugation (*25*), gel filtration, and electron microscopy (*24*). The conversion of protofibrils to fibrils is sudden and can be seeded by preformed Aβ fibrils but not by preformed Aβ protofibrils (*18*). Furthermore, Aβ40 solutions preincubated to form longer protofibrils (up to ca. 200 nm long) convert to fibrils after addition of fibrillar seeds approximately twice as rapidly as freshly prepared solutions containing shorter protofibrils (ca. 50 nm or less) (*18*). This finding suggests that the process of Aβ protofibril elongation and assembly may be a critical one in the disease process. Recently, protofibril-like species have also been observed during fibril formation by other disease-associated proteins including the islet amyloid polypeptide (IAPP) (*26*), transthyretin (*27*), α-synuclein (*28*), and acyl phosphatase (which is amyloidogenic but not associated with disease) (*29*). We report herein detailed studies of Aβ protofibril assembly and disassembly, as well as preliminary studies of these species using carbon nanotube AFM tips.

MATERIALS AND METHODS

Synthetic Aβ Peptides. Aβ40 and Aβ42 were purchased from Quality Controlled Biochemicals Inc. (Hopkinton, MA).

Seed-free Aβ40/Aβ42 stock solutions in dimethyl sulfoxide (DMSO) were prepared at concentrations of 12−15 mg/mL. The solution was sonicated (5−10 min in a Branson 1200 water bath sonicator) and filtered through a 0.2 μm nylon microspin filter to remove any undissolved seed. Final peptide concentrations of the DMSO stock solutions, as determined by quantitative amino acid analysis, were typically 2−2.5 mM.

Initiation of in vitro aggregation of Aβ40/42 was accomplished by adding an aliquot of a concentrated DMSO stock of Aβ40 to aqueous buffer (10 mM phosphate, 137 mM NaCl, and 27 mM KCl, pH 7.4, unless otherwise specified) followed by immediate vortexing to mix thoroughly. For experiments investigating the concentration dependence of protofibril elongation, [DMSO] in the aggregation buffer was kept constant (≤10 vol %). After initial mixing, the solutions were incubated at room temperature without further agitation except for the removal of aliquots for AFM analysis. Solutions used to investigate the effect of glycerol were prepared without presolubilization in DMSO. Instead, Aβ40 was solubilized at alkaline pH using NaOH solutions before adding buffer to neutralize the solution and generate an aqueous stock solution. Briefly, the peptide was taken up with enough NaOH to titrate the solution to pH 8−9 (with 10 mM NaOH) at which point the solution cleared. After sonicating for 2 min, concentrated buffer was added to create an aqueous Aβ40 stock at pH 7.4 (10 mM phosphate, 100 mM NaCl) which was stored at −20 °C until use.

AFM Specimen Preparation. Aliquots of 3−5 μL were removed from peptide incubations and placed on freshly cleaved mica. After incubating (30 s to 2 min), the remaining suspension was removed by rinsing (twice with 50 μL of water) to remove salt and loosely bound peptide. Excess water was removed with a gentle stream of difluoroethane (Dust-Off Plus, Falcon Safety Products Inc.), and the samples were stored in a covered container to protect them from contamination until they were imaged (within 1−2 h).

Optimization of Protofibril Adsorption Density. For accurate length measurements, specimens with dispersed protofibrils were produced by diluting the samples at 15−25 μM between 30 s and 2 min prior to specimen preparation. The amount of dilution and the incubation time were kept constant within each series of measurements (see below).

Atomic Force Microscopy. All images were obtained under ambient conditions with a Nanoscope IIIa Multimode scanning probe workstation (Digital Instruments, Santa Barbara, CA) operating in TappingMode using etched silicon NanoProbes (probe model FESP, Digital Instruments). Scanning parameters varied with individual tips and samples, but typical ranges were as follows: initial root-mean-square amplitude, 1.6 V; setpoint, 1.1−1.4 V; tapping frequency, 70−90 kHz; scan rate, 1.5−2 Hz. Consecutive scans were monitored until distortion due to creep or shifts in the slow scan direction were negligible before collecting scans at sizes of 1 μm with the maximum 512 × 512 pixel resolution (occasionally 2 μm scan sizes were used when protofibril adsorption density was too low to find 50 protofibrils in a 1 μm square region).

Preparation and Application of Carbon Nanotube AFM Tips. Carbon nanotube tips were fabricated as reported earlier (*20*).

Counting Adsorbed Species and Measurement of Average Protofibril Length and Longest Protofibril. Protofibrils were measured in fields containing 50−100 assemblies by summing the lengths of short line segments (in top view mode in the Nanoscope software) to approximate the curvature of protofibrils. Globular aggregates measuring <20 nm and showing no evidence of elongation were counted in each region and included in the calculation of average protofibril length as described below. Only protofibrils that could clearly be distinguished (including ∼4 nm high globular aggregates, which were assumed to be roughly spherical, with diameter = length = 4.3 nm) were included in the average. Before calculating the average, 8.5 nm was subtracted from the length of the elongated features to compensate for the contribution of tip-related broadening artifacts [calculated by subtracting the approximate protofibril height (4.3 nm) from the average protofibril width measured at half-height (12.8 ± 2.5 nm)] (*20*). The adjusted lengths were summed

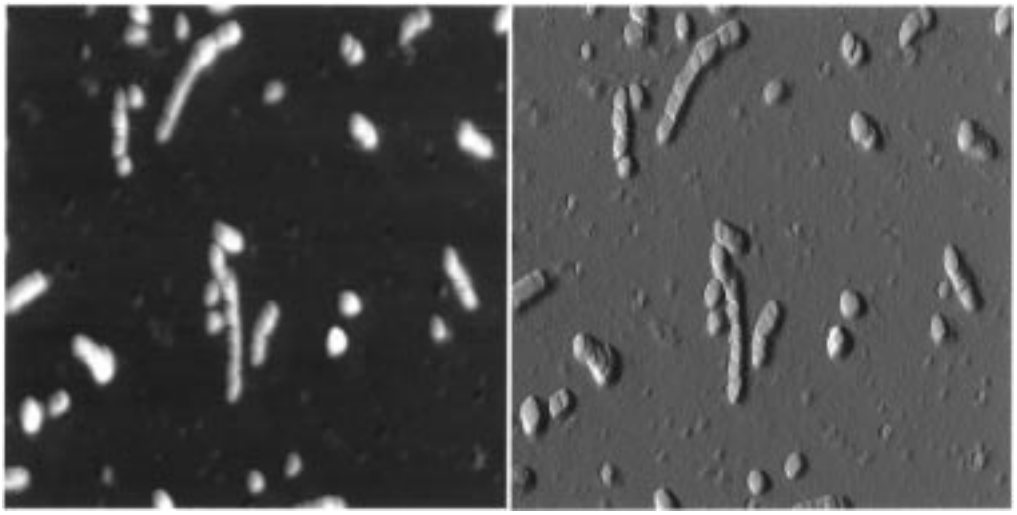

FIGURE 1: AFM images of Aβ40 protofibrils obtained with a carbon nanotube probe (*20*). The images are 500 × 500 nm and were collected simultaneously in height mode (left, where increasing brightness corresponds to increasing feature height), and amplitude mode (right, where increasing brightness indicates greater damping of cantilever oscillation). "Spherical" assemblies and the 20 nm periodicity of height increases along the axis of the protofibril can be clearly distinguished in these images.

and divided by the number of protofibrils to yield the average protofibril length. Typical scans were 1 μm square scans captured at highest resolution (512 × 512 pixels), giving a pixel size of ~2 nm. The estimated error of ±5 nm listed for protofibril average length measurements is based in part on the ±2 pixel error of each measurement. To measure the longest protofibril, each field was divided into quadrants and the longest protofibril present in each was measured. The average length of the longest protofibrils in each quadrant plus or minus the standard deviation is presented as the longest protofibril in the sample.

Brief Dilution Does Not Affect Measured Protofibril Lengths. After 7 and 22 days of incubation (average temperature = 18 °C), aliquots of an Aβ40 solution (32 μM) were used to make specimens either without dilution or following brief (≤30 s) dilution to 16 μM. The average protofibril length and the length of the longest protofibril were not affected by this procedure.

RESULTS

Following Aβ Protofibril Formation and Elongation by Atomic Force Microscopy. Atomic force microscopy (AFM) has proven to be a valuable technique for following amyloid fibril formation (*30*). Since precise, detailed three-dimensional information can be obtained, AFM analysis provides the capability to simultaneously distinguish and characterize multiple adsorbed species that vary greatly in size. This capability enables detailed analysis of subtle changes in aggregate species over time but does not provide information about changes in nonadsorbing species (monomer, etc.), so AFM analysis cannot address changes in overall mass balance between monomeric and aggregate species in solution. In fact, size-exclusion chromatography analysis of Aβ protofibril formation by Walsh et al. indicates that protofibril intermediates account for only a small portion (larger for Aβ42 than for Aβ40, but always <50% of total peptide in each case) of peptide present at any given time during fibril formation by Aβ40 and Aβ42 (*24*) even though they are the major species observed by AFM prior to the initiation of fibril formation. The processes of protofibril initiation and protofibril elongation are distinct, and it may be possible to influence them separately, so it is important to have methods capable of distinguishing and measuring each process. The AFM measurements presented herein seek to provide insight into factors that influence elongation of individual protofibrils.

Sample aliquots were removed from an incubation at regular intervals and adsorbed to an atomically smooth mica surface (*18, 19*). To ensure that all of the predominant oligomeric species were being detected on mica surfaces, identical aliquots were also adsorbed onto oxidized graphite (HOPG) surfaces, which are known to have very different adsorption characteristics. All of the species reported herein, albeit in smaller quantities, *and no additional species* were observed on HOPG, suggesting that the predominant intermediates were detected (*19*). Thus, changes in the abundance of observable species over time are likely to be relevant to the actual process.

Aβ40 Protofibril Periodicity Was Clearly Seen in Nanotube Images. Aβ40 protofibrils, imaged with carbon nanotube tips (*20*), coexisted with spherical species (ca. 3.9 ± 0.5 nm diameter for both) that may represent assembly subunits (see below). Longer protofibrils were characterized by a clearly periodic substructure, spaced at ca. 20 nm intervals along the Aβ40 protofibril axis (Figure 1). As reported earlier (*20*), the difference between the maximum and minimum heights along the axis was at least 1 nm.

Aβ40 protofibril assembly was quantified using three features of the observed population: the number of adsorbed protofibrils, the average length of these protofibrils, and the longest adsorbed protofibril as described in detail in the Materials and Methods. The number of protofibrils depends on the balance between their initiation, disassembly (see below), and incorporation into larger aggregates. In contrast, the length measurements were intended to isolate the elongation process. Changes in average protofibril length do *not* provide an accurate representation of protofibril elongation if the number of protofibrils changes during the measurement period, if protofibrils are prone to disassembly episodes during growth (as is the case for microtubules) (*31, 32*), or if a subpopulation of protofibrils becomes dormant

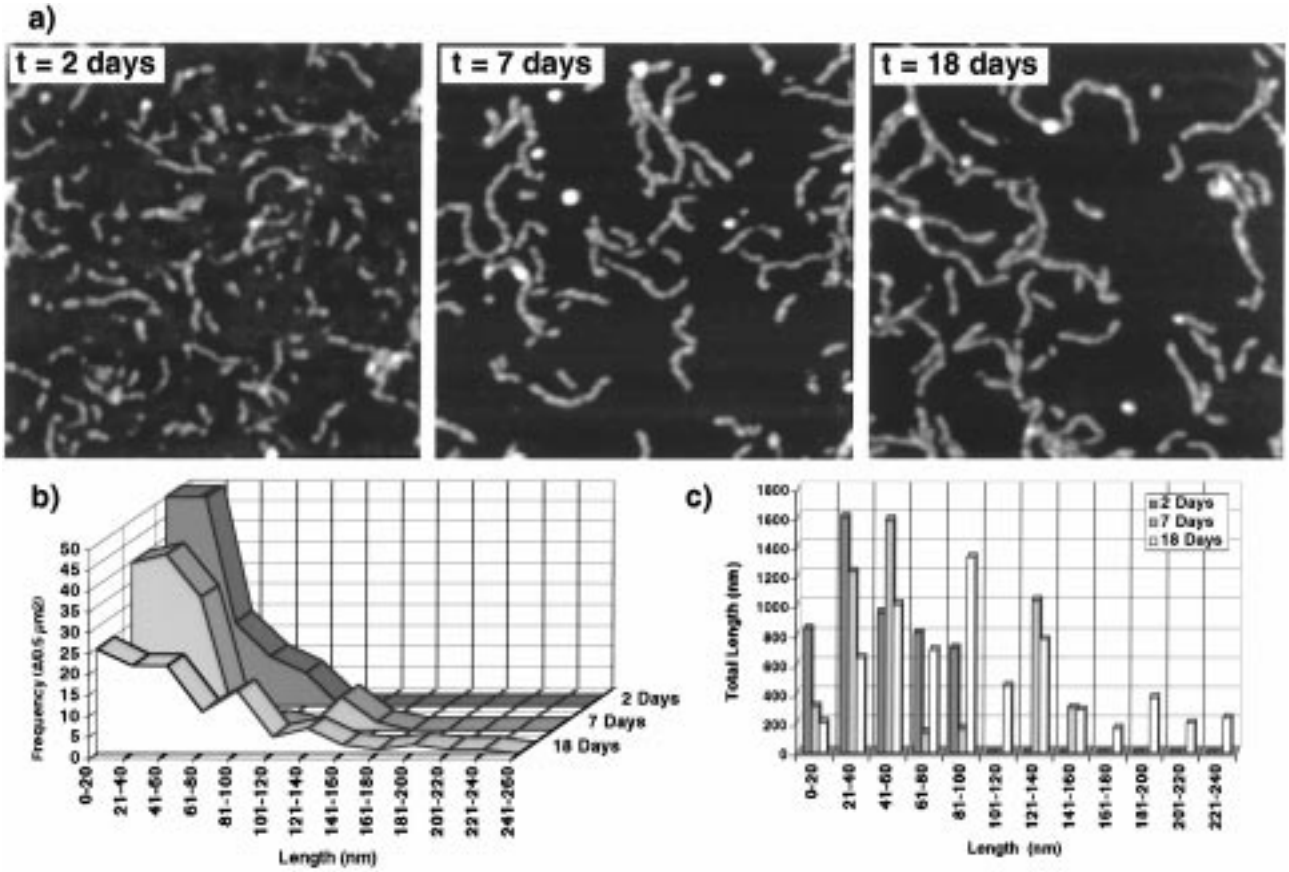

FIGURE 2: Time dependence of Aβ40 protofibril assembly. (a) AFM images (500 × 500 nm) at 2, 7, and 18 days. (b) Histograms reflecting the population of protofibrils within 20 nm length ranges found in 0.5 μm^2 regions including the images shown above. With increasing time the population of longer protofibrils increased while the population of the shortest protofibrils decreased (note: there were greater than 50 species/0.5 μm^2 in the smaller length categories at day 2 (124 features 0−20 nm long and 56 features 21−40 nm long), but the histogram was truncated to allow better comparison of the longer length categories at the three time points). Total protofibril density (species per squared micrometer field on mica surface) decreased over time from 440 at day two to 256 at day seven to 218 at day 18. (c) Histograms reflecting the relative mass of peptide (estimated by comparing the total length of protofibrils in that length range) represented by protofibrils in each length range. The length range accounting for the greatest mass of peptide increased steadily with time as the amount of Aβ in the shortest protofibrils decreased.

while others continue to grow (an analogous scenario has been described for in vitro elongation of *salmonella* flagella) (*33*). We report herein that the number of protofibrils in a given field (or protofibril density) changes during a typical incubation, complicating the interpretation of average lengths. In contrast, the longest protofibril measurement is not dependent on the number of adsorbed protofibrils.

Aβ40 Protofibrils Elongate and Become Less Numerous Over Time. A 100 μM Aβ40 solution was incubated at room temperature, and aliquots were periodically removed for AFM imaging. The images and histograms shown in Figure 2 show that with increasing time, the length of the adsorbed Aβ40 protofibrils increased and the relative mass of adsorbed peptide (estimated by the total length of protofibrils in each length range) in the form of longer protofibrils increased. Protofibrils longer than 100 nm were observed with greater frequency (ca. 1% of protofibrils at 2 days, 8% after 7 days and 20% after 18 days) while short protofibrils ($\leq$40 nm) remained common (Figure 2b). At the same time, the protofibril length range accounting for the greatest amount of deposited Aβ shifted from 21 to 40 nm at 2 days to 41−60 nm after 7 days and 81−100 nm after 18 days (Figure 2c). The average height of the Aβ40 protofibrils (ca. 4 nm) did not change significantly with time, indicating that growth occurs primarily, if not entirely, by addition of Aβ40 to the ends of protofibrils.

While the length of the observed protofibrils increased, the number of adsorbed species in a given area clearly decreased (see Figures 2 and 3). The correlation between decreasing density and increasing length was seen in all of the assembly experiments discussed herein. This correlation suggests that small protofibrils may coalesce end-to-end; although, these results cannot rule out the possibility that the spherical assembly could be a rapidly formed, off-pathway reservoir for Aβ that is consumed over time as protofibrils deplete free Aβ (*34*). However, the height match of the small spherical species with the elongated protofibrils and in situ AFM observations of growing Aβ protofibrils reported recently by Kowalewski et al. (*21*) suggest that the spherical Aβ species are incorporated directly.

Elongation of Protofibrils Depends on Aβ40 Concentration. Elongation of Aβ40 protofibrils was measured as a function of Aβ40 concentration (16, 32, 80, and 160 μM, see Figure 3). The rate of protofibril elongation measured both by average protofibril length and length of the longest protofibril (see Materials and Methods for details) increased with increasing Aβ40 concentration. At 16 and 32 μM, the maximum length reached a plateau between 2 and 5 days,

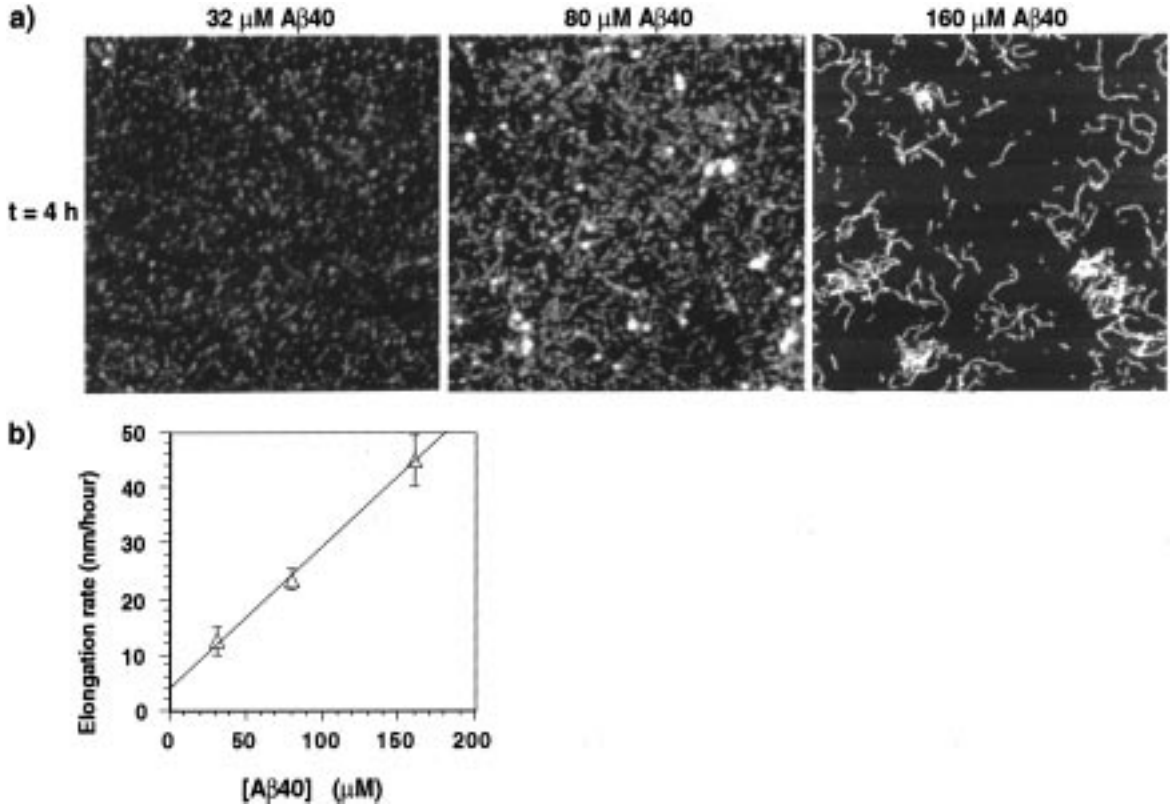

FIGURE 3: Concentration dependence of Aβ40 protofibril assembly. (a) AFM images of specimens prepared from Aβ40 solutions incubated at the indicated concentrations for 4 h at room temperature (all images are 1 μm $\times$ 1 μm). The 80 and 160 μM samples were briefly diluted to 16 μM just prior to specimen preparation to adjust protofibril density so that lengths could be measured (see Materials and Methods). (b) Elongation rate based on longest protofibril in each sample after 4 h vs [Aβ40] ($R^2 = 0.998$).

suggesting that the critical concentration of Aβ40 had been reached in the solution [previous estimates of the critical concentration were 10−40 μM (*17*)]. The initial elongation rate was calculated based on the longest protofibril present at $t = 4$ h (50 $\pm$ 10.6 nm for the 32 μM incubation, 94 $\pm$ 7.9 nm at 80 μM, and 179 $\pm$ 19.2 nm at 160 μM). The measured rate at $t = 4$ h varied between 10 nm/h at 32 μM and 45 nm/h at 160 μM and was a linear ($R^2 = 0.998$) function, first-order in [Aβ40] (Figure 3b). The linear dependence of initial protofibril growth rates on Aβ40 concentration is consistent with sequential addition of Aβ40 being the rate-determining step during the initial stages of protofibril elongation. Once sufficient populations of short protofibrils are formed, growth by condensation of short protofibrils can also contribute to elongation (see above and ref *21*).

Elongation rates calculated using average protofibril length yielded smaller values and were not linearly related to [Aβ40] ($R^2 = 0.907$). Elongation rates calculated based on increases in maximum protofibril length between later time points decreased with increasing time (approximately 10−20-fold reduction in elongation rates comparing initial rate over 4 h to subsequent growth over the next 2 days). The density of observable species decreased with increasing Aβ40 concentration, reflecting the fact that the 80 μM and 160 μM incubations were diluted to 16 μM prior to adsorption in order to allow more accurate comparisons of protofibril lengths to be made (see Figure 3).

Aβ40 and Aβ42 Protofibril Elongation Rates Are Comparable. Aβ42 protofibril elongation was followed at concentrations of 15, 25, and 50 μM. The average elongation rate over the first 24 h varied between 2 and 5 nm/h. This average rate is comparable to the rate of Aβ40 protofibril elongation when calculated over a similar period, but ca. 10-fold slower than Aβ40 protofibril elongation averaged over the first 4 h of growth (see above).

Disassembly Occurs on Dilution of Aβ40 Protofibrils. After aggregation of a solution of Aβ40 (160 μM) at 18 °C for 4 h, the sample was diluted 20-fold (to [Aβ40] = 8 μM) and the incubation was analyzed by AFM at $t = 0$, 25 min, 3 days, and 7 days (Figure 4). Resulting changes in the lengths of protofibrils were measured by the average protofibril length and length of the longest protofibril, both of which decreased slowly over time. The disassembly rate at 8 μM was -24 ± 7.3 nm/day through day 3, compared to the assembly rate at 32 μM which was 40 $\pm$ 4.4 nm/day through day 2 and 19 $\pm$ 1.4 nm/day through 7 days (these measurements were based on length of longest protofibril). Significantly, the density of adsorbed species decreased along with the length measurements (124/μm^2 at $t = 0$, 103 at 3 days, and 52 at 7 days). The observation that the rate of decrease in protofibril length was much faster over the first 3 days as compared to the subsequent 4 (see Figure 4) is consistent with an equilibrium between disassembly and assembly (i.e., the critical concentration) being reached at an Aβ40 concentration less than 8 μM. This is slightly lower than previously published estimates of the critical concentration of Aβ40 which vary from 10 to 40 μM (*17*).

Aβ Protofibril Elongation Is Temperature Dependent. Protofibril elongation was monitored in identical solutions of Aβ40 (100 μM), which were incubated at 3, 18, and 37 °C. AFM images of these samples revealed obvious

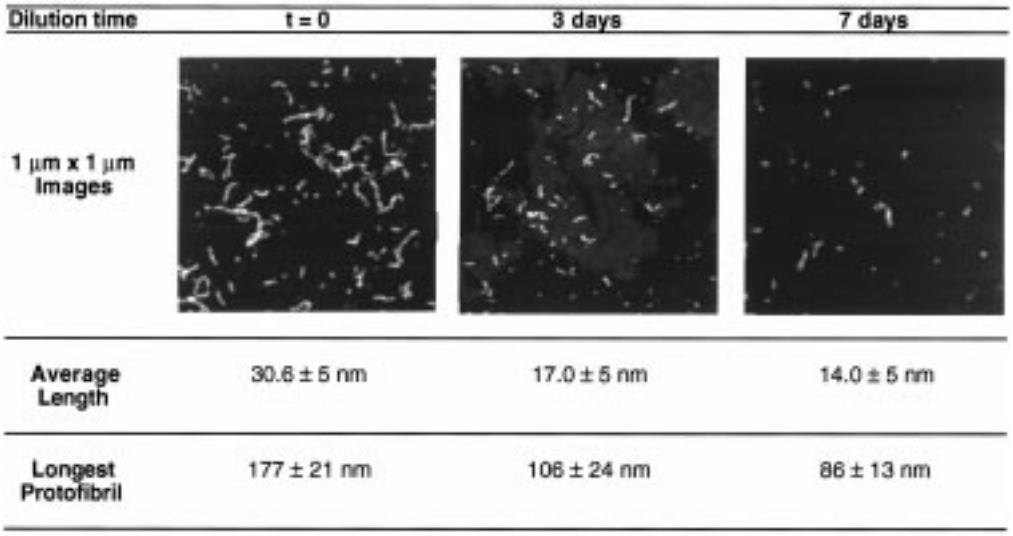

FIGURE 4: Effect of extended dilution on protofibril lengths. An Aβ40 solution (160 μM, $t = 4$ h) containing protofibrils was diluted to 8 μM and protofibril lengths were analyzed at the indicated times following dilution.

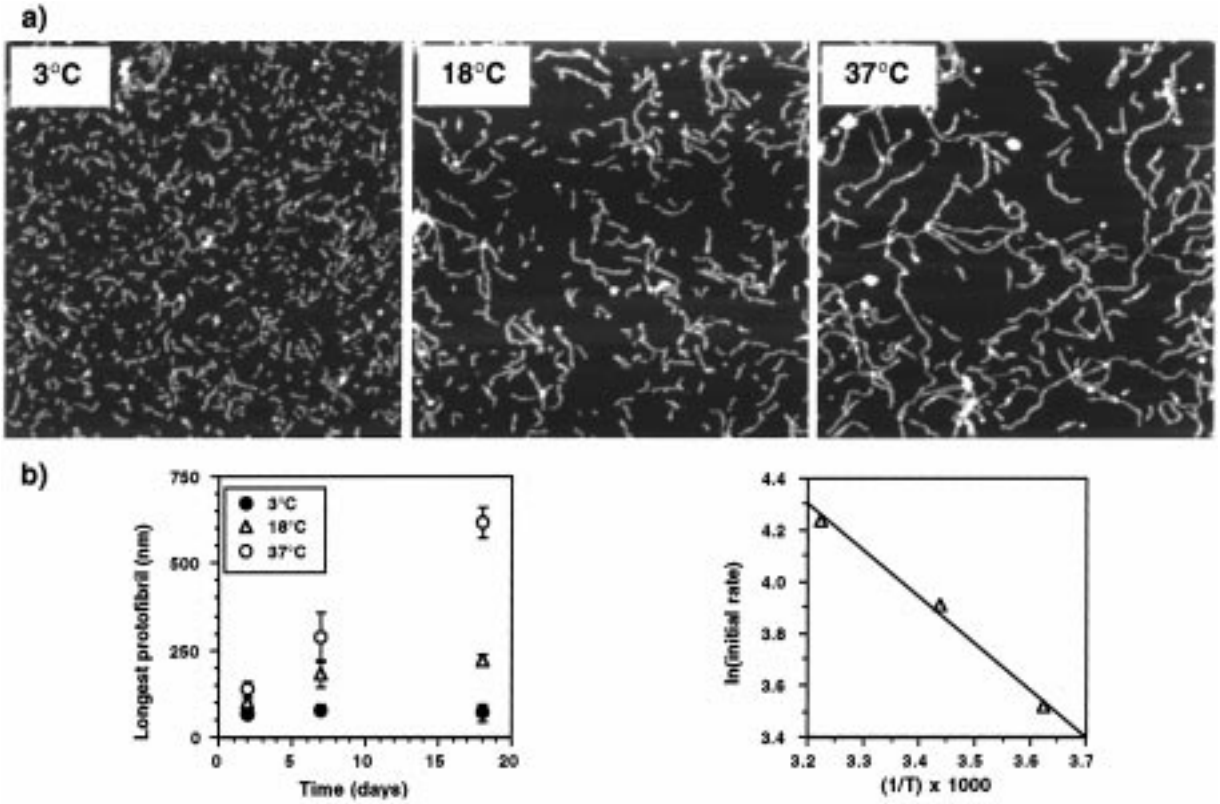

FIGURE 5: Temperature dependence of Aβ40 protofibril assembly. (a) AFM images of Aβ40 protofibrils grown at different temperatures. Parallel solutions containing 100 μM total Aβ40 were incubated for 7 days at the temperature indicated. All images are 1 μm square. (b) Temperature dependence of protofibril growth based on longest protofibril method. (Left) Length of longest protofibril vs time. (Right) Arrhenius plot based on longest protofibril at $t = 2$ days for each temperature. $R^2 = 0.993$.

increases in protofibril length with increasing temperature at each time point examined (Figure 5). This change is not due to differences in sample preparation or adsorption (controls not shown). Figure 5b shows that a plot of the natural log of the average growth rates based on maximum lengths versus the reciprocal of the absolute incubation temperature is linear over the temperature range studied. As was the case in the concentration-dependence study, the maximum protofibril length method (Figure 5) provided a much more accurate fit ($R^2 = 0.993$) than did the average length method ($R^2 = 0.94$). The number of adsorbed species decreased with time at every temperature and decreased with increasing temperature at fixed concentrations (species per squared micrometer at 3 °C, 1004 at 2d, 816 at 7d, 453 at 18d; at 18 °C, 440 at 2d, 256 at 7d, 218 at 18d; at 37 °C, 224 at 2d, 146 at 7d, 46 at 18d).

Aβ Protofibril Elongation Is Accelerated by Increasing Concentrations of Sodium Chloride. Aggregation of 100 μM Aβ40 at room temperature was followed in 100 mM phosphate buffer (pH 7.4) containing increasing amounts of NaCl (0, 50, 100, or 500 millimolar added NaCl). The density of protofibrils adsorbed to mica during preparation of parallel

control specimens was observed to increase with increasing [NaCl], consistent with previous investigations of the effect of [NaCl] on the adsorption of amyloid fibrils formed by IAPP (*35*). However, there were no changes in protofibril length distribution in these controls as a result of changes in the adsorption density (data not shown). Therefore, differences in length among aggregating solutions reflect altered assembly rather than adsorption-related artifacts. For the experimental aggregations, there was very little evidence of aggregation in the absence of added NaCl; protofibrils were only observed after ≥7 days and then only occasionally (~5 protofibrils/μm^2, lengths of ≤50 nm). In contrast, numerous protofibrils were seen after 2 days in the solutions containing 50 and 100 mM NaCl. Finally, at 500 mM NaCl, protofibrils observed at early time points formed large mats. Average protofibril lengths and protofibril growth rates increased significantly with NaCl concentration (data not shown).

Aβ Protofibril Elongation Is pH Dependent. We compared the aggregation of 50 μM Aβ40 at pH 1.0 (0.1 N HCl, used previously in dynamic light scattering investigations of fibril growth kinetics) (*36*), pH 4.5 (10 mM acetate-buffered saline), pH 5.8 (10 mM MES-buffered saline) (*37*), and pH 7.4 (10 mM phosphate-buffered saline) (saline = 137 mM NaCl, 27 mM KCl). The pH 1.0 sample contained long filaments (lengths commonly of ≥1 μm with diameters of 3−4 nm) that showed little evidence of association/clumping. In contrast, the samples at pH 4.5 and 5.8 both produced specimens characterized by very large masses of material (often as large as 5 μm) that displayed features extending from their periphery that closely resembled protofibrils, not fibrils (images not shown). In all cases, the appearance of the aggregates formed differed significantly from the fibrils formed in phosphate-buffered saline at pH 7.4. Because of the rapid formation of very long, thin filaments at pH 1 and the association of protofibrils into large masses at pH 4.5 and 5.8, it was not possible to measure protofibril elongation rates under these conditions.

Aβ Protofibril Elongation Is Promoted by Glycerol. On the basis of a report of its acceleration of Aβ fibril formation (P. Fraser, personal communication), glycerol (10−50 vol % in 10% increments) was included in a series of 37 °C incubations that were analyzed at 18 and 48 h. For these experiments, the Aβ40 solutions were prepared by initially solubilizing the Aβ40 at alkaline pH with sonication before addition of buffer to produce DMSO-free aggregation solutions. In all cases, the protofibrils displayed the same morphology as seen in DMSO-containing solutions. Protofibril lengths were significantly longer at all time points in solutions containing ≥20% glycerol compared to those without glycerol or those containing 10% glycerol. At 22 days, the samples incubated in 10−30% glycerol contained fibrils, as did the control incubation without glycerol. However, the samples incubated in 40 and 50% glycerol contained only protofibrils. Thus, fibril formation can be inhibited under conditions which promote protofibril formation. This divergent effect of glycerol on protofibril vs fibril growth demonstrates that the two assembly processes are distinct and can be selectively influenced by a single agent.

DISCUSSION

Aβ Amyloid Fibril Formation Is a Multistage Process. It is critical to understand the process of amyloid fibril formation in order to understand the pathogenesis of AD and to select a specific target for therapeutic intervention. The observation of the Aβ protofibril, a transient intermediate in amyloid fibril assembly (*18, 19, 24*), demonstrates the importance of using multiple complementary methods, since the failure to detect it previously had led to the incorrect assumption that fibril formation involved a cooperative (intermediate-free) transition of unstructured Aβ monomer to Aβ fibril (*17*). Although additional mechanistic studies remain to be done, recent studies, including those reported herein, suggest four stages of amyloid fibril assembly. (1) Protofibril initiation may be a nucleation-dependent event and may require fewer than 20 Aβ molecules, judging from the approximate volume of the earliest protofibrils. This step has been shown by Walsh et al. (*24*) (using gel filtration chromatography to separate Aβ monomer and protofibril) to be accelerated for Aβ42 as compared to Aβ40. (2) Protofibril elongation, followed herein, may involve coalescence of smaller protofibrils (*21*). Aβ42 and Aβ40 protofibrils elongate at comparable rates, although it should be emphasized that a slight difference, undetectable by the in vitro AFM method discussed herein, may be critical in vivo. Protofibril assembly is reversible on dilution, and disassembly may occur by a different process than protofibril growth. (3) Protofibril-to-fibril transition appears to be the cooperative step, involving protofibril association, winding, and possibly, a conformational change (*18*). This is the first step that is easily detected by turbidity and dye-binding assays. This step does not appear to be easily reversible—once protofibrils disappear during fibril formation they do not reappear, even on dilution of fibrils. (4) Fibril elongation can be initiated by the addition of preformed fibrillar seeds to an Aβ monomer or protofibril solution (*18, 38*). Rates of fibril elongation are comparable for Aβ42 and Aβ40 (*38*). Thus, the faster rate of Aβ42 amyloid fibril formation compared to Aβ40 that was first detected in a crude turbidity assay (*6*) may primarily be due to increased initiation of Aβ42 protofibrils and/or acceleration of the subsequent conversion to fibrils.

No Single Method Can Detect and Quantify All Intermediates. Because multiple distinct small globular species are observed by AFM, monitoring of protofibril elongation should ideally be accompanied by measurement of changes in the quantity of each species. Several techniques, including analytical ultracentrifugation analysis (*39*) and mass spectrometry, which have the potential to separate and quantitate the species present in aggregating incubations of Aβ, may be able to provide these measurements. Aβ amyloid fibril formation has been followed by several methods which detect the fibril either indirectly, using probes such as thioflavin T (detects enhanced fluorescence emission intensity) or Congo Red (UV shift detected on binding), or directly, by the changed solubility (*40*), turbidity (*6*), hydrodynamic radius [gel filtration (*24*) and QLS (*36*)], or density [analytical ultracentrifugation (*25*)] of the Aβ protein. Although these methods provide useful descriptions of temporal changes, none can be interpreted in structural or morphological terms without additional data from complementary techniques (*17*). In addition, the existence of discrete oligomeric species cannot be easily detected. It is important to note that the Aβ protofibril appears to be soluble; it is not easily sedimented,

is too small to produce turbidity, and may not have fibril-like dye-binding properties.

Atomic Force Microscopy Allows the Observation of Individual Oligomeric Aβ Assemblies and Allows Ordered Fibrillar Species To Be Distinguished from Amorphous Aβ Aggregates. Atomic force microscopy provides quantitative three-dimensional morphological information unavailable via standard electron microscopy. The Aβ protofibril was not distinguished from fibrils in electron microscopic studies because its width was not clearly distinguishable from that of the fibril. In contrast, AFM allowed the protofibril to be easily distinguished by its height: approximately 40% that of the fibril (*19*). In addition, Walsh et al. were able to separate protofibrils from fibrils and monomeric Aβ by sedimentation followed by gel filtration chromatography (*24*). The ability to observe individual assemblies by AFM, as opposed to measuring their average properties, allowed various conditions that had been reported to promote Aβ aggregation to be compared. For example, previous investigations of Aβ aggregation as a function of pH indicated that maximal aggregation in unseeded Aβ40 solutions [as determined by detection of beta sheet (*41, 42*), turbidity (*25*), Congo red binding (*37*), and thioflavin T binding (*37, 43*)] occurs between pH 5 and 6. However, Wetzel and coworkers demonstrated that aggregates formed at pH 5.8, in contrast to fibrils formed at pH 7.4, were amorphous and sometimes appeared in electron micrographs as large (widths in the 100 nm range) bundles of small filaments (*37*). In addition, the aggregate formed at pH 5.8 was unable to seed fibril formation at pH 7.4 and did not convert to fibrils when the sample was adjusted to pH 7.4 (*37*). We have confirmed that aggregation at pH 5.8 (and at pH 4.5) does not primarily produce fibrillar assemblies. In fact, the determination that Aβ aggregates formed at pH 4.5 and 5.8 are largely protofibrillar explains the inability of these aggregates to seed fibril formation (*18, 37*).

Protofibril Elongation, Like Fibril Elongation, Is First-Order in [Aβ]. The growth of Aβ fibrils, seeded by preexisting fibrils, has been determined to be first-order in [Aβ40], measured by several methods (*38, 43*−*45*). Protofibril elongation is also first-order in [Aβ]. Although this first-order relationship is consistent with protofibril growth by sequential addition of monomeric Aβ to growing protofibril ends, the inverse relationship between length of protofibrils and number of protofibrils suggests that the process is more complex—possibly including protofibril growth by coalescence of existing protofibrils (*21*). The concentration dependence of protofibril elongation may result from direct participation of Aβ in the protofibril coalescence or from the concentration dependent formation of Aβ photofibrils. This latter quantity cannot be measured by AFM as reported herein, but could possibly be estimated by gel filtration chromatography combined with amino acid analysis for Aβ quantitation. In contrast to assembly, the disassembly of protofibrils does *not* result in an apparent increase in the number of protofibrils; when diluted, the decrease in Aβ40 protofibril length is paralleled by a decrease in the number of adsorbed species. The simplest explanation for this observation is that protofibril disassembly may occur via a different mechanism than protofibril assembly. For example, the growth process may involve addition of both monomeric Aβ and coalescence of smaller protofibrils, while disassembly releases only monomeric Aβ. In this scenario, monomer association would be the only reversible equilibrium process, and protofibril coalescence would be an irreversible growth step.

Protofibril Elongation Is Promoted by Elevated Temperatures. Although more detailed kinetic studies are clearly needed in order to fully understand the mechanism of protofibril elongation, it is worth noting two interesting observations. First, protofibril elongation is promoted by increased temperature, which is known to promote unfolding of globular proteins. Second, elongation is promoted by increased concentrations of salt and glycerol, which accelerate protofibril elongation, are known to *disfavor* unfolding of globular proteins. These observations, which may owe to the "hydrophobic effect", are the subject of continuing studies. It should be noted that under conditions where protofibril formation is not clearly seen (pH 1), a more pronounced promoting effect of increased temperature was measured for the process of fibril elongation (*46*).

The Protofibril Rather Than The Fibril Itself May Be the Optimal Target for Drug Discovery Efforts. One practical outcome of the determination of the mechanism of assembly of Aβ amyloid fibrils is that a potential AD therapeutic target could be elucidated (*14*). In that regard, it is important to remember that it is the *process* of Aβ fibrillogenesis, *not* the Aβ amyloid fibril itself, that is linked by circumstantial evidence to AD pathogenesis (*5, 15*). Thus, compounds that inhibit Aβ fibril formation may, by allowing certain intermediates to accumulate, actually promote pathogenesis (*15*). Six recent papers support the idea that nonfibrillar oligomeric Aβ species are pathogenic (1) Nonfibrillar "spherical" 4.8−5.7 nm diameter Aβ42 species, designated Aβ-derived diffusible ligands (ADDLs) (*13*), are toxic to cultured neurons via a discrete receptor-mediated pathway and inhibit LTP in tissue slices. The dimensions of ADDLs are consistent with those measured herein for the earliest Aβ42 protofibrils, taking into account reported differences in AFM conditions. (2) Oligomeric, Aβ-derived species have been detected in the cerebrospinal fluid of AD patients, but not in age-matched controls, by fluorescence correlation microscopy (*47*). (3) The brains of very young Down syndrome patients, who are destined to develop AD (and amyloid) in their thirties, contain significant amounts of deposited (aggregated), but nonfibrillar Aβ42 (*4*). (4) Behavioral and cognitive defects exhibited by different APP transgenic mouse lines arise prior to the formation of amyloid plaques (*48, 49*). (5) Although time-dependent self-assembly of Aβ is clearly required for several of its in vitro activities, one such activity has been observed to diminish over time, suggesting that an intermediate oligomeric species may be active (*50*). (6) The most effective peptidyl inhibitors of Aβ in vitro neurotoxicity actually increase the rate of its fibrillization (as measured by dynamic light scattering) and alter the fibril morphology (*51*). Ultimately, clinical trials of amyloid inhibitors will provide the first unambiguous experimental test of whether Aβ-ordered aggregation causes AD or is merely an epiphenomenon associated with neuronal degeneration. Given the possibility that fibril precursors such as protofibrils may actually be the pathogenic species, it will be critical to select inhibitors of the early stages of Aβ oligomerization for these trials.

ACKNOWLEDGMENT

We thank Dominic Walsh, Tomas Ding, Youcef Fezoui, and David Teplow for valuable discussions. We also thank Paul Fraser for sharing his results regarding the effects of glycerol on fibril formation prior to its publication.

REFERENCES

1. Lansbury, P. T., Jr. (1996) *Acc. Chem. Res. 29*, 317−321.
2. Rumble, B., Retallack, R., Hilbich, C., Simms, G., Multhaup, G., Martins, R., Hockey, A., Montgomery, P., Beyreuther, K., and Masters, C. L. (1989) *N. Engl. J. Med. 320*, 1446−1452.
3. Cummings, B. J., Pike, C. J., Shankle, R., and Cotman, C. W. (1996) *Neurobiol. Aging 17*, 921−933.
4. Lemere, C. A., Blustzajn, J. K., Yamaguchi, H., Wisniewski, T., Saido, T. C., and Selkoe, D. J. (1996) *Neurobiol. Dis. 3*, 16−32.
5. Selkoe, D. (1997) *Science 275*, 630−631.
6. Jarrett, J. T., Berger, E. P., and Lansbury, P. T., Jr. (1993) *Biochemistry 32*, 4693−4697.
7. Corder, E. H., Saunders, A. M., Strittmatter, W. J., Schmechel, D. E., Gaskell Jr., P. C., Small, G. W., Roses, A. D., Haines, J. L., and Pericak-Vance, M. A. (1993) *Science 261*, 921−923.
8. Schmechel, D. E., Saunders, A. M., Strittmatter, W. J., Crain, B. J., Hulette, C. M., Joo, S. H., Pericak-Vance, M. A., Goldgaber, D., and Roses, A. D. (1993) *Proc. Natl. Acad. Sci. U.S.A. 90*, 9649−9653.
9. Hyman, B. T., West, H. L., Rebeck, G. W., Buldyrev, S. V., Mantegna, R. N., Ukleja, M., Havlin, S., and Stanley, H. E. (1995) *Proc. Natl. Acad. Sci. U.S.A. 92*, 3586−3590.
10. Lippa, C. F., Smith, T. W., Saunders, A. M., Crook, R., Pulaski-Salo, D., Davies, P., Hardy, J., Roses, A. D., and Dickson, D. (1995) *Neurology 45*, 97−103.
11. Raby, C. A., Morganti-Kossmann, M. C., Kossmann, T., Stahel, P. F., Watson, M. D., Evans, L. M., Mehta, P. D., Spiegel, K., Kuo, Y. M., Roher, A. E., and Emmerling, M. R. (1998) *J. Neurochem. 71*, 2505−2509.
12. Smith, D. H., Nakamura, M., McIntosh, T. K., Wang, J., Rodriguez, A., Chen, X. H., Raghupathi, R., Saatman, K. E., Clemens, J., Schmidt, M. L., Lee, V. M., and Trojanowski, J. Q. (1998) *Am. J. Pathol. 153*, 1005−1010.
13. Lambert, M. P., Barlow, A. K., Chromy, B. A., Edwards, C., Freed, R., Liosatos, M., Morgan, T. E., Rozovsky, I., Trommer, B., Viola, K. L., Wals, P., Zhang, C., Finch, C. E., Krafft, G. A., and Klein, W. L. (1998) *Proc. Natl. Acad. Sci. U.S.A. 95*, 6448−6453.
14. Lansbury, P. T., Jr. (1997) *Curr. Opin. Chem. Biol. 1*, 260−267.
15. Lansbury, P. T., Jr. (1999) *Proc. Natl. Acad. Sci. U.S.A. 96*, 3342−3344.
16. Jarrett, J. T., and Lansbury, P T., Jr. (1993) *Cell 73*, 1055−1058.
17. Harper, J. D., and Lansbury, P. T., Jr. (1997) *Annu. Rev. Biochem. 66*, 385−407.
18. Harper, J. D., Lieber, C. M., and Lansbury, P. T., Jr. (1997) *Chem. Biol. 4*, 951−959.
19. Harper, J. D., Wong, S. S., Lieber, C. M., and Lansbury, P. T., Jr. (1997) *Chem. Biol. 4*, 119−125.
20. Wong, S. S., Harper, J. D., Lansbury, P. T., Jr., and Lieber, C. M. (1998) *J. Am. Chem. Soc. 120*, 603−604.
21. Kowalewski, T., and Holtzman, D. M. (1999) *Proc. Natl. Acad. Sci. U.S.A. 96*, 3688−3693.
22. Hansma, H. G., and Hoh, J. H. (1994) *Annu. Rev. Biophys. Biomol. Struct. 23*, 115−139.
23. Bustamante, C., and Keller, D. (1995) *Phys. Today* 32−38.
24. Walsh, D. M., Lomakin, A., Benedek, G. B., Condron, M. M., and Teplow, D. B. (1997) *J. Biol. Chem. 272*, 22364−22372.
25. Snyder, S. W., Ladror, U. S., Wade, W. S., Wang, G. T., Barrett, L. W., Matayoski, E. D., J, H. H., Krafft, G., and Holzman, T. (1994) *Biophys. J. 67*, 1216−1228.
26. Goldsbury, C., Kistler, J., Aebi, U., Arvinte, T., and Cooper, G. J. S. (1999) *J. Mol. Biol. 285*, 33−39.
27. Lashuel, H. A., Lai, Z., and Kelley, J. W. (1998) *Biochemistry 37*, 17851−17864.
28. Conway, K., Harper, J., and Lansbury, P. T., Jr. (1998) *Nat. Med. 4*, 1318−1320.
29. Chiti, F., Webster, P., Taddei, N., Clark, A., Stefani, M., Ramponi, G., and Dobson, C. M. (1999) *Proc. Natl. Acad. Sci. U.S.A. 96*, 3590−3594.
30. Ding, T. T., and Harper, J. D. (1999) *Methods Enzymol. 309* (in press).
31. Mitchison, T., and Kirschner, M. (1984) *Nature 312*, 237−242.
32. Walker, R. A., O'Brien, E. T., Pryer, N. K., Soboeiero, M. F., Voter, W. A., Erickson, H. P., and Salmon, E. D. (1988) *J. Cell. Biol. 107*, 1437−1448.
33. Hotani, H., and Asakura, S. (1974) *J. Mol. Biol. 86*, 285−300.
34. Lomakin, A., Teplow, D. B., Kirschner, D. A., and Benedek, G. B. (1997) *Proc. Natl. Acad. Sci. U.S.A. 94*, 7942−7947.
35. Müller, D. J., Amrein, M., and Engel, A. (1997) *J. Struct. Biol. 119*, 172−188.
36. Lomakin, A., Chung, D. S., Benedek, G. B., Kirschner, D. A., and Teplow, D. B. (1996) *Proc. Natl. Acad. Sci. U.S.A. 93*, 1125−1129.
37. Wood, S. J., Maleeff, B., Hart, T., and Wetzel, R. (1996) *J. Mol. Biol. 256*, 870−877.
38. Naiki, H., Hasegawa, K., Yamaguchi, I., Nakamura, H., Gejyo, F., and Nakakuki, K. (1998) *Biochemistry 37*, 17882−17889.
39. Schuck, P., MacPhee, C. E., and Howlett, G. J. (1998) *Biophys. J. 74*, 466−474.
40. Maggio, J. E., Stimson, E. R., Ghilardi, J. R., Allen, C. J., Dahl, C. E., Whitcomb, D. C., Vigna, S. R., Vinters, H. V., Labenski, M. E., and Mantyh, P. W. (1992) *Proc. Natl. Acad. Sci. U.S.A. 89*, 5462−5466.
41. Barrow, C. J., and Zagorski, M. G. (1991) *Science 253*, 179−182.
42. Barrow, C. J., Yasuda, A., Kenny, P. T. M., and Zagorski, M. G. (1992) *J. Mol. Biol. 225*, 1075−1093.
43. Naiki, H., and Nakakuki, K. (1996) *Lab. Invest. 74*, 374−383.
44. Esler, W. P., Stimson, E. R., Ghilardi, J. R., Vinters, H. V., Lee, J. P., Mantyh, P. W., and Maggio, J. E. (1996) *Biochemistry 35*, 749−757.
45. Esler, W. P., Stimson, E. R., Ghilardi, J. R., Felix, A. M., Lu, Y.-A., Vinters, H. V., Mantyh, P. W., and Maggio, J. E. (1997) *Nat. Biotech. 15*, 258−263.
46. Kusumoto, Y., Lomakin, A., Teplow, D. B., and Benedek, G. B. (1998) *Proc. Natl. Acad. Sci. U.S.A. 95*, 12277−12282.
47. Pitschke, M., Prior, R., Haupt, M., and Riesner, D. (1998) *Nat. Med. 4*, 832−834.
48. Moechars, D., Dewachter, I., Lorent, K., Reversé, K., Baekelandt, V., Naidu, A., Tesseur, I., Spittaels, K., Van Den Haute, C., Checler, F., Godaux, E., Cordell, B., and Van Leuven, F. (1999) *J. Biol. Chem. 274*, 6483−6492.
49. Hsia, A. Y., Masliah, E., McConlogue, L., Yu, G. Q., Tatsuno, G., Hu, K., Kholodenko, D., Malenka, R. C., Nicoll, R. C., and Mucke, L. (1999) *Proc. Natl. Acad. Sci. U.S.A. 96*, 3228−3233.
50. Crawford, F., Soto, C., Suo, Z., Fang, C., Parker, T., Sawar, A., Frangione, B., and Mullan, M. (1998) *FEBS Lett. 436*, 445−448.
51. Pallitto, M. M., Ghanta, J., Heinzelman, P., Kiessling, L. L., and Murphy, R. M. (1999) *Biochemistry 38*, 3570−3578.

BI9904149